# Electronic supplement to the paper "The dam-break problem for concentrated suspensions of neutrally buoyant particles"

C. ANCEY, N. ANDREINI, AND G. EPELY–CHAUVIN,

Environmental Hydraulics Laboratory,
École Polytechnique Fédérale de Lausanne, 1015 Lausanne, Switzerland

(Received February 2013)

The objective of this electronic supplement is to provide further information on the experimental protocol and calculations presented in the body of our paper. In parallel, we also present two movies that can give a better idea of the experimental setup and conditions.

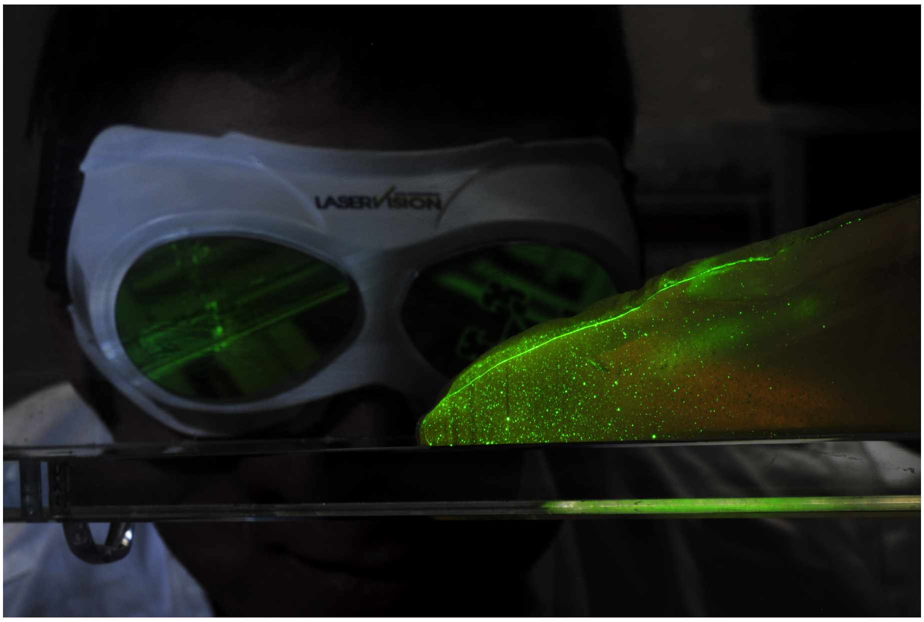


A dam break experiment being conducted: a laser beam illuminates the front area of the flowing suspension. Actually, we worked in darkness.

# 1. Theoretical developments

## 1.1. *Sidewall effect*

Here, we are interested in calculating the position of the front as a function of time in the presence of sidewalls. For this purpose, we will use the kinematic wave approximation. We assume that the flow velocity accommodates instantaneously to any change in the flow depth. Everything happens as if the flow were locally steady and uniform. In this case, the momentum equation reduces to a balance between the bottom shear stress and gravitational forces. To take sidewall friction into account, we utilize the Darcy-Weisbach formula. Chow (1959) showed that for viscous fluids in open channel flows, the mean bottom shear stress can be expressed in dimensional form as

$$\hat{\tau}_b = \frac{1}{8} f \rho \bar{u}^2 = 3\mu \left(1 + 2\frac{h}{W}\right) \frac{\hat{U}}{\hat{h}}, \tag{1.1}$$

where the Darcy-Weisbach friction factor $f$ is expressed as $f = 24/Re_h$ with $Re_h = \rho \hat{U} \hat{R}_h/\mu$ the generalized Reynolds number and $\hat{R}_h = Wh/(W + 2h)$ the hydraulic radius (where $W$ denotes the flume width). $\hat{U}$ denotes the depth-averaged velocity. For a steady uniform flow, we have $\hat{\tau}_b = \rho g \hat{R}_h \sin\theta$, from which we deduce that in dimensionless form, the cross-section averaged velocity is

$$U = \frac{1}{3} \frac{h^2}{(1 + 2\epsilon_w h)^2}, \tag{1.2}$$

where $\epsilon_w = H_*/W$ is the typical depth-to-width ratio. Mass conservation implies that

$$\frac{\partial h}{\partial t} + \frac{\partial U h}{\partial x} = 0, \tag{1.3}$$

subject to the boundary conditions

$$\int_0^{x_f(t)} h(x,t)dx = 1 \text{ and } h(x_f) = 0. \tag{1.4}$$

We seek solutions in the form of expansions

$$h(x,t) = h_0(x,t) + \epsilon_w h_1(x,t) + \epsilon_w^2 h_2(x,t) + \cdots \text{ and } x_f(t) = x_{f,0}(t) + \epsilon_w x_{f,1}(t) + \epsilon_w^2 x_{f,2}(t) + \cdots \tag{1.5}$$

Volume conservation implies

order $\epsilon^0$ $$\int_0^{x_{f,0}} h_0(x,t)\,dx = 1 \tag{1.6}$$

order $\epsilon^1$ $$\int_0^{x_{f,0}} h_1(x,t)\,dx + h_0(x_{f,0},t)x_{f,1} = 0 \tag{1.7}$$

order $\epsilon^2$ $$\int_0^{x_{f,0}} h_2(x,t)\,dx + h_1(x_{f,0},t)x_{f,1} + h_0(x_{f,0},t)x_{f,2} + \frac{1}{2}x_{f,1}^2 \partial_x h_0(x_{f,0},t) = 0 \tag{1.8}$$

To order $\epsilon^0$, the governing equation (1.3) reduces to $\partial_t h_0 + h_0^2 \partial_x h_0 = 0$, which is easily solved:

$$h_0(x,t) = \sqrt{\frac{x}{t}} \text{ and } x_{f,0} = \left(\frac{9}{4}t\right)^{1/3} \tag{1.9}$$

To order $\epsilon^1$, the governing equation is $\partial_t h_1 + t^{-1}\partial_x(xh_1) = 8x/(3t^2)$, whose solutions are

$$h_1(x,t) = \frac{8}{3}\frac{x}{t} \text{ and } x_{f,1} = -2 \tag{1.10}$$

To order $\epsilon^2$, we get $\partial_t h_2 + t^{-1}\partial_x(xh_2) = 70x^{3/2}/(9t^{5/2})$, whose solutions are

$$h_2(x,t) = \frac{70}{9}\left(\frac{x}{t}\right)^{3/2} \text{ and } x_{f,2} = \frac{35}{3}\left(\frac{2}{3t^2}\right)^{1/3} + 2\left(\frac{12}{t^2}\right)^{1/3} \tag{1.11}$$

### 1.2. *Suspension balance model*

Another approach to particle migration is the so-called *suspension balance model*, which leads to a relation between the particle flux and the divergence of the particle stress tensor $\mathbf{\Sigma}^p$ (Nott & Brady 1994; Morris & Boulay 1999; Miller *et al.* 2009)

$$\boldsymbol{j} = -f(\phi)\frac{2}{9}\frac{\epsilon_a^2}{\epsilon}\boldsymbol{\nabla}\cdot\mathbf{\Sigma}^p, \tag{1.12}$$

where $f(\phi)$ denotes the mean mobility of the particle phase (that is, the sedimentation hindrance function given, for instance, by the Richardson and Zaki law) and the particle stress tensor is the sum of the viscous stress tensor and a term that accounts for the stress anisotropy (nonzero normal stress differences)

$$\mathbf{\Sigma}^p = 2\frac{\eta_p(\phi)}{\bar{\eta}}\boldsymbol{d} - \frac{\eta_n(\phi)}{\bar{\eta}}\dot{\gamma}\boldsymbol{Q} \tag{1.13}$$

where we have introduced

$$\eta_p(\phi)+1 = \eta(\phi),\, \eta_n(\phi) = K_n\left(\frac{\phi}{\phi_m}\right)^2\left(1-\frac{\phi}{\phi_m}\right)^{-2} \text{ and } \boldsymbol{Q} = \begin{pmatrix} \lambda_1 & 0 & 0 \\ 0 & \lambda_2 & 0 \\ 0 & 0 & \lambda_3 \end{pmatrix}. \tag{1.14}$$

There, $K_n$ is a constant called the normal stress viscosity, $\lambda_i$ are the normal stress coefficients (in the flow direction, $\lambda_i = 1$ and in the other directions $\lambda_j \neq 1$), $\boldsymbol{d}$ is the strain rate tensor, and $\dot{\gamma} = \sqrt{2\boldsymbol{d} : \boldsymbol{d}}$ is the second invariant of the strain rate tensor, with the stress scale $\Sigma_* = \mu(\bar{\phi})U_*/H_* = \mu_f\bar{\eta}U_*/H_*$.

The respective merits of the shear-induced migration and suspension balance models have been identified in light of various experiments, most of them conducted on rotating geometries (Couette, parallel-plate, cone-and-plate rheometers). For moderately concentrated suspensions in Couette flows, both approaches predict the shear rate and particle concentration profiles reasonably well (Shapley *et al.* 2004; Ovarlez *et al.* 2006) and none of them appears to have a significant advantage over the other. These experimental campaigns also provided evidence that the theoretical results are quite sensitive to the parameters used in their formulation, more specifically the maximum solid fraction $\phi_m$ and the exponent $\beta$ in the Krieger-Dougherty relation : $\eta(\phi) = (1-\phi/\phi_m)^{-\beta}$. On rare occasions, channel flows and axisymmetric Poiseuille flows have been used to compare both approaches (Koh *et al.* 1994; Hampton *et al.* 1997; Lyon & Leal 1998*a*,*b*; Norman *et al.* 2005).

Here emphasis is given to flows down an inclined plane. For the steady state solution ($\boldsymbol{j} = 0$), the normal component $\Sigma^p_{yy}$ of the particle stress tensor should be constant throughout the depth. For a film of homogeneous fluid, this constant is zero in the absence of surface tension effects, but here, as demonstrated by Timberlake & Morris (2005), we expect a stress jump at the free surface as a result of such effects. This is because on one hand, the free surface may be slightly convex for flows down narrow flumes and, on the other hand, the capillary normal forces of the fluid phase resist the protrusion of particles into the free boundary. We then set $\Sigma^p_{yy} = \lambda_2\eta_n(\phi)\dot{\gamma} = c$, which

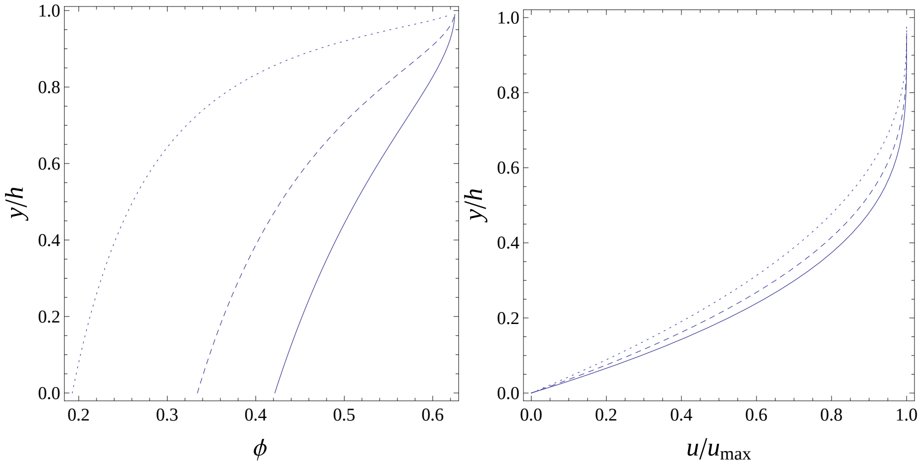


FIGURE 1. Particle concentration and velocity profiles predicted by (1.16) for three mean concentrations $\bar{\phi} = 30\%$ (dashed line), $\bar{\phi} = 45\%$ (dotted line), and $\bar{\phi} = 52\%$ (solid line). The Krieger-Dougherty relation has been used with $\beta = 1.82$.

in conjunction with the shear-rate equation [equation (2.14) in the paper]

$$\dot{\gamma} = \frac{\bar{\eta}}{\eta(\phi)}(h-y), \tag{1.15}$$

provides

$$\left(\frac{\phi}{\phi_m}\right)^2 \left(1-\frac{\phi}{\phi_m}\right)^{\beta-2} = \frac{c}{\lambda_2 K_n \bar{\eta}} \frac{1}{h-y}, \tag{1.16}$$

from which we deduce that we must have $\beta < 2$ for the solution to be comparable with that worked out using the shear-induced migration model (i.e., flow sheared across the whole depth). Some authors such as Krieger (1972) have suggested that $\beta = 1.82$. For $\beta \geqslant 2$, we have $\phi \to \phi_m$ when $y \to h$, so that the suspension reaches a jammed state: the basal layer is sheared, but the upper flow region is rigid. This plug flow is reminiscent of viscoplastic flows, but here the unyielding region originates from particle migration rather than colloidal interactions. Such rigid regions have been observed in wide-gap Couette rheometers (Ovarlez *et al.* 2006; Wiederseiner 2010).

As does the shear-induced diffusion model, the suspension balance model predicts that the higher the concentration is, the blunter the velocity profile. Figure 1 shows a typical example of the velocity and concentration profiles obtained by solving equation (1.16) numerically. The constant of integration $c$ was adjusted so that the depth-averaged value of $\phi$ matches the mean particle concentration. This procedure may seem peculiar as this constant $c$ was related to a boundary condition on the stress flux at the free boundary. From the qualitative viewpoint, a comparison with the shear-induced diffusion model (compare with figure 2 in the paper) does not reveal significant differences between the concentration and velocity profiles except that, with the suspension balance model, $\phi$ can reach $\phi_m$ if we select $\beta \geqslant 2$ (see above) whereas $\phi_m$ is reached at the free surface when using the shear-induced diffusion model. We have estimated the degree of blunting by adjusting a power-law function to fit the numerical velocity data. Figure 2 below shows the variation in $n$ with the mean particle concentration for the two models. The dependence of $n$ on $\phi$ is similar to that observed with the shear-induced diffusion model for the set of parameters $\beta$ and $\phi_m$ used here.

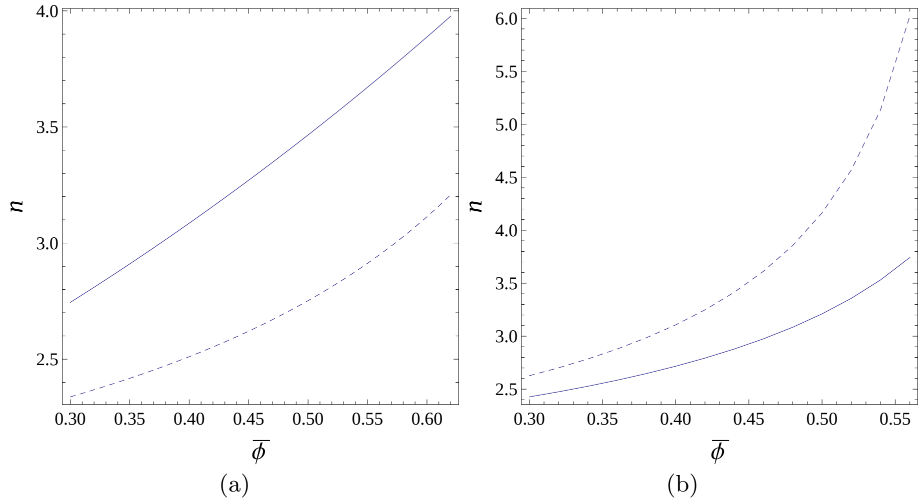


FIGURE 2. Variation in the blunting index $n$ as a function of the mean particle concentration. (a): the $n$ values were determined by fitting a power-law function on the velocity profile using the shear-induced diffusion model with $\beta = 2$ and $\alpha = 3/2$ (solid line) or $\beta = 2$ and $\alpha = 1.042\phi + 0.1142$ (dashed line). (b): the $n$ values were determined by fitting a power-law function on the velocity profile using the suspension balance approach and equation (1.16) with $\beta = 1.82$ (dashed line) or $\beta = 1.5$ (solid line).

## 2. Experimental protocol

### 2.1. *Suspension composition*

All experiments (except for one) were run with concentrated suspensions of poly(methyl methacrylate) (PMMA) particles within a mixture of fluids called *trimix*, which was prepared so that the suspension was isodense (the density mismatch between the fluid and solid phases was zero to within $5 \times 10^{-4}$ g cm$^{-3}$) and isoindex (the particles and fluids had the same refractive index to within $10^{-4}$), as explained in § 2.2. Preparing a transparent suspension of neutrally buoyant particles is a complicated process, which requires considerable attention at every step.

We used PMMA particles, manufactured by Altuglass (la Garenne-Colombes, France). All particles used in our experiments came from a single batch. As the raw material was polydisperse (particle size ranging from 15 μm to 475 μm), we sieved it using a sieving machine (Retsch AS200 Control) with a 180 μm sealed sieving stack. The mean particle diameter was then 190 μm (standard deviation 60 μm). The resulting distribution was bell-shaped. Material choice was dictated by many criteria: the greatest clarity of the suspension (the suspension must be transparent over a few centimeters) (Wiederseiner *et al.* 2011), the absence of microstructure effects due to layering seen in some particle migration experiments (Bricker & Butler 2006; Deshpande & Shapley 2010) (hence a slightly polydisperse particle suspension), and the lowest price (several kilograms were needed).

### 2.2. *Suspension preparation and handling*

To match the refractive index and the density of the particles at the same time, we used a mixture with three components, called *trimix*. We adapted the fluid mixture composition originally described by Lyon & Leal (1998*a*). The particle density and refractive index were matched by a fluid mixture with mass fractions of 50% Triton X100, 28% 1,6-Dibromohexane (DBH), and 22% UCON oil (75-H450 oil from Dow Chemicals). Each of these components imparted a distinctive feature to the mixture: the Triton X100 enabled high refractive index, DBH made it possible to adjust the density, and by using different UCON oils, we could adapt the fluid viscosity within a relatively wide range. The final mixture density was $\rho = 1.184 \pm 5 \times 10^{-4}$ g/cm$^3$, the refractive index was measured using an Atago rx5000a refractometer at 532 nm and 20 °C: we found $n_r = 1.4885 \pm 2 \times 10^{-4}$. The viscosity was measured using a Bohlin CVOR rheometer equipped with a cone and plate geometry: we found $\mu_f = 0.124 \pm 3 \times 10^{-3}$ Pa s at 20 °C. The surface tension was measured using the pendant drop method (Hansen & Rødsrud 1991): we found $\sigma = 33 \pm 5$ mN m$^{-1}$. The uncertainty concerning the bulk density resulted from various processes (e.g., errors in the temperature control, errors in the fluid-density measurements).

A few problems arose in the preparation of the suspension, such as air bubbles trapped in the suspension and the absorbtion of small quantities of water vapour (up to 0.2% of the total mass), which markedly changed the refractive index of trimix. We proceeded as follows to eliminate both problems (Andreini 2012). We first prepared 15 kg of suspension by vigorously stirring particles and trimix at the desired concentration $\phi$ by hand. A small amount of rhodamine (fluorescent dye that reacts when excited by the laser beam) was added to differentiate the fluid and particle phases. The suspension was then left for one night in a sealed cylindrical container and stirred at 50 rpm with a 6-blade propeller, which made it possible to obtain a homogenous suspension (the particle concentration and temperature were homogeneous throughout the suspension). At the same time, a vacuum pump reduced the air pressure to 20 mb in the container, which was sufficient to remove all air bubbles and water. At the end of the outgassing process, the suspension temperature was a few degrees too high for the suspension to be transparent. While still stirring the suspension to homogenize temperature, we finally cooled the sealed container with a thermal bath until the suspension temperature dropped to $20 \pm 0.05$ °C and the refractive index of the trimix matched that of particles. The cooling process lasted a couple of hours. The suspension was then ready. During the flume experiments, the suspension was exposed to the ambient air and thus absorbed water vapour. The degassing process had to be repeated prior to each run.

### 2.3. *Measurement systems*

We measured different flow variables (e.g., front position, flow depth), but the emphasis was given to flow visualization. We measured the velocity profiles in the direction normal to the flume bottom and, with less success, particle concentration profiles using high-speed cameras and particle image velocimetry (PIV) techniques. For PIV measurements, we used a Basler A504k camera working at 200 to 1270 Hz (depending on front velocity), mounted with a Nikkor 105 mm macro lens with an aperture of f/4. The images were then processed using classic PIV techniques (Raffel *et al.* 2007). Velocity fields were computed using the open source software called MatPIV (Sveen 2004). Particle concentrations were estimated by counting the number of coarse particles contained in a given slice, but the estimation was quite poor because of the image quality and resolution, as explained below.

Figure 3 explains how we measured velocity profiles. Taking images from the side was possible with uniform flows, but much more restrictive from the optical standpoint for nonuniform flows. For instance, filming from the side did not allow measurement of velocities within the head far from the sidewall due to the strong curvature of the free surface. Moreover, as we used a fairly wide flume and measured profiles along the centerline (5 cm from the sidewall), we needed to be able to see through 5 cm of suspension, i.e., approximately 1000 fluid-particle interfaces, which went beyond the current capacities (Wiederseiner *et al.* 2011). The idea was then to film from below the flume bottom. Due

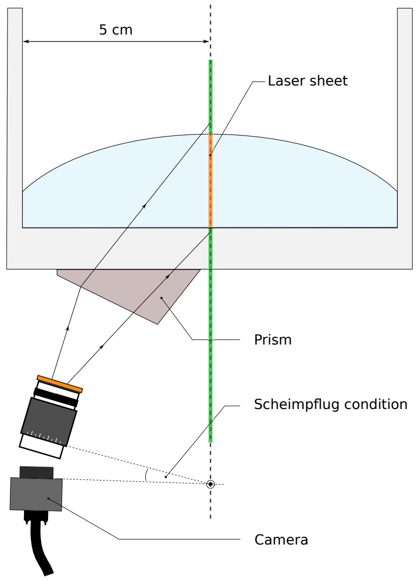


FIGURE 3. (Colour online). Sketch of the measurement system for the velocity profiles within the moving suspension. Because of the suspension/air interface and the three-dimensional nature of the flows, we were forced to film the flow from below. When taking images with a camera whose sensor (CCD) is not parallel with the object, one can use the Scheimpflug principle, which involves tilting the camera until the image plane (on the CCD), the lens plane, and the object plane (lit by the laser sheet) have a common line of intersection (see chap. 7 in Raffel *et al.* (2007) for additional information).

to the much shorter optical path, the images were of much better quality and were not altered by the curvature of the free surface. This technique had, however, the disadvantage of producing blurred and distorted images if no corrective action were taken. To get around this problem, we adjusted the inclinations of the camera CCD and the lens so that the Scheimpflug rule was satisfied (the image was then in focus). A prism (made up of a PMMA block, with the same refractive index as that of the flume bottom) was also needed to avoid refraction. As this system caused significant image distortion, we had to correct it to compute the velocity field properly; this was done by taking an image of a test chart and using the Matlab built-in function *cp2tform* to undistort the images. Figure 4 shows a typical raw image of the front that we used in our treatment, while figure 5 shows a perspective view of the front lit by the laser plane.

The particle concentration was estimated by counting the number of particles inside a given window, then taking the time average. The typical window size was $700 \times 20$ px$^2$, i.e. $35 \times 1$ mm$^2$ and the time length over which integration was performed was 100 images, i.e. from 0.08 to 0.40 s. Among the various procedures tested, this technique gave the best results in terms of reproducibility and robustness. However, it performed well only for a thin region along the flume bottom. When approaching the free surface, image quality deteriorated significantly as a result of accumulating problems. The most significant issue was that when taking images from below, the optical path was not constant, but increased linearly with the distance to the bottom (as shown in figure 3 with the two parallel rays through the flume). This means that the number of particle interfaces (each of which introduced a slight amount of refraction) crossed by the rays increased away from the bottom, which induced a significant loss of clarity throughout the depth. Typically, for a flow depth of 2 cm and rays inclined at 30 deg to the bottom,

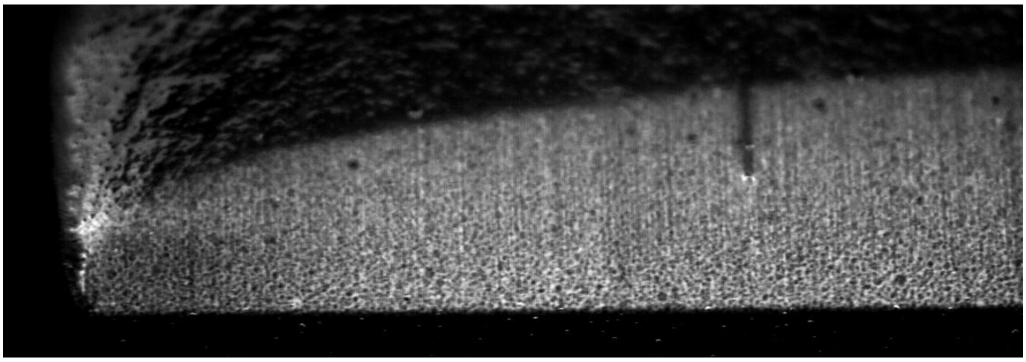

FIGURE 4. Typical raw image taken by the camera from the bottom of the flume (flow from right to left). The black dots are the PMMA particles whereas the white area is produced by the rhodamine contained in the fluid. The corrugated free surface can be distinguished at the top of the picture and near the front, the vertical thick black line on the right of the image was due to a small bubble trapped within the flow. The picture was taken at the centerline of the flume, the solids fraction was $\phi = 52\%$, and the flow depth $\sim 1.5$ cm.

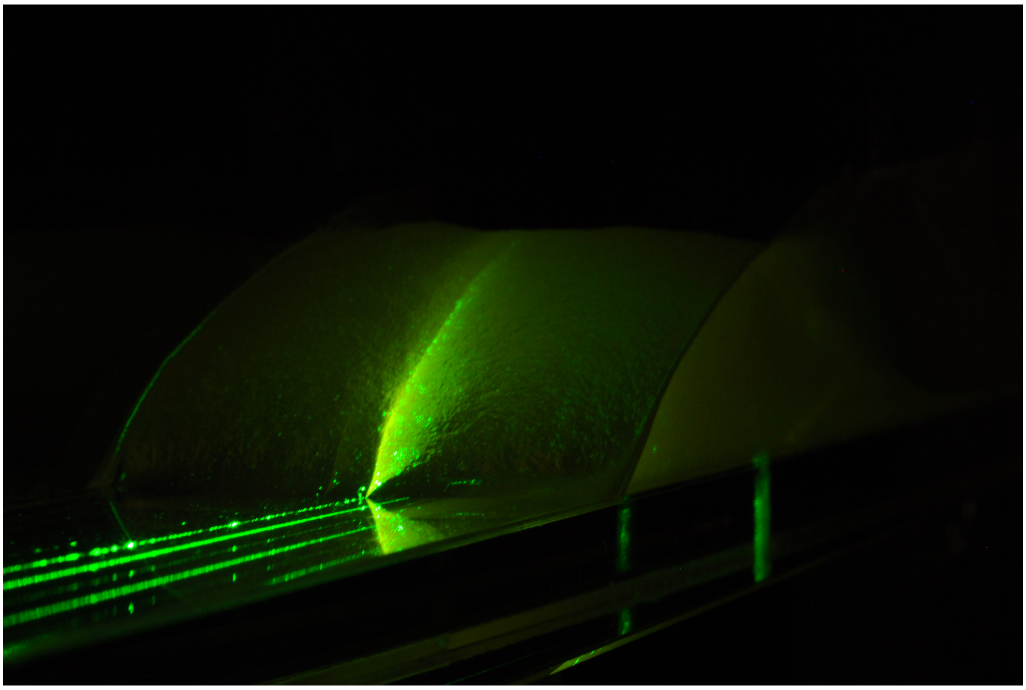

FIGURE 5. View of the front area cut by the laser plane.

the number of particles encountered was as large as $20/(\sin 30 d_p) \sim 200$, with $d_p = 0.2$ mm the mean particle diameter. Another issue was related to the widening of the laser sheet from the flow base to free surface. When approaching the free surface, the laser sheet was likely to be wider than one particle diameter, which made it difficult to clearly distinguish between particles. Relative uncertainties on local $\phi$ measurements did not exceeded 2% for $\hat{y} \leqslant 60$ px and 4% for $60 \leqslant \hat{y} \leqslant 80$ px, but increased tremendously for $\hat{y} > 100$ px.

## 3. movies

Movie 1: this movie shows the flowing suspension from above. Note the parabolic shape of the contact line.

Movie 2: this movie shows a side view of the flowing suspension taken from the sidewall, 2.5 m downstream of the flume inlet. Flow from right to left. Suspension: solids fraction of 0.52; flume inclination 25°. Note that the raw images, which were subsequently used for the treatment, were not taken from the sidewall, but from below (see figure 3). The black dots are the PMMA particles whereas the white area is produced by the rhodamine contained in the fluid and whose fluorescence is excited by the laser.

### REFERENCES


Andreini, N. 2012 Dam break of Newtoniam fluids and granular suspensions: Internal dynamics measurements. PhD thesis, Ecole Polytechnique Fédérale de Lausanne.

Bricker, J. & Butler, J.E. 2006 Oscillatory shear of suspensions of noncolloidal particles. *J. Rheol.* **50**, 711–728.

Chow, V.T., ed. 1959 *Open-Channel Hydraulics*. New York: Mc Graw Hill.

Deshpande, K.V. & Shapley, N.C. 2010 Particle migration in oscillatory torsional flows of concentrated suspensions. *J. Rheol.* **54**, 663–686.

Hampton, R.E., Mammoli, A.A., Graham, A.L. & Tetlow, N. 1997 Migration of particles undergoing pressure-driven flow in a circular conduit. *J. Rheol.* **41** (621-640).

Hansen, F.K. & Rødsrud, G. 1991 Surface tension by pendant drop: I. A fast standard instrument using computer image analysis. *J. Colloid. Interface Sci.* **141**, 1–9.

Koh, C.J., Hookham, P. & Leal, L.G. 1994 An experimental investigation of concentrated suspension flows in a rectangular channel. *J. Fluid Mech.* **266**, 1–32.

Krieger, I.M. 1972 Rheology of monodispersed lattices. *Adv. Colloid Interface Sci.* **3**, 111–136.

Lyon, M.K. & Leal, L.G. 1998*a* An experimental study of the motion of concentrated suspensions in two-dimensional channel flow. Part 1. Monodisperse systems. *J. Fluid Mech.* **363**, 25–56.

Lyon, M.K. & Leal, L.G. 1998*b* An experimental study of the motion of concentrated suspensions in two-dimensional channel flow. Part 2. Bidisperse systems. *J. Fluid Mech.* **363**, 57–77.

Miller, R.M., Singh, J.P. & Morris, J.F. 2009 Suspension flow modeling for general geometries. *Chem. Eng. Sci.* **64**, 4597–4610.

Morris, J.F. & Boulay, F. 1999 Curvilinear flows of noncolloidal suspensions: the role of normal stresses. *J. Rheol.* **43**, 1213–1238.

Norman, J.T., Nayak, H.V. & Bonnecaze, R.T. 2005 Migration of buoyant particles in low-Reynolds-number pressure-driven flows. *J. Fluid Mech.* **523**, 1–35.

Nott, P.R. & Brady, J.F 1994 Pressure-driven flow of suspensions: simulation and theory. *J. Fluid Mech.* **275**, 157–199.

Ovarlez, G., Bertrand, F. & Rodts, S. 2006 Local determination of the constitutive law of a dense suspension of noncolloidal particles through magnetic resonance imaging. *J. Rheol.* **50**, 259–292.

Raffel, M., Willert, C.E., Wereley, S.T. & Kompenhans, J. 2007 *Particle Image Velocimetry*. Berlin: Springer.

Shapley, N.C., Brown, R.A. & Armstrong, R.C. 2004 Evaluation of particle migration models based on laser Doppler velocimetry measurements in concentrated suspensions. *J. Rheol.* **48**, 255–279.

Sveen, J.K. 2004 An introduction to MatPIV. *Tech. Rep.* eprint series No. 2 “Mechanics and Applied Mathematics” ISSN 0809-4403. Department of Mathematics, University of Oslo,.

Timberlake, B.D. & Morris, J.F. 2005 Particle migration and free-surface topography in inclined plane flow of a suspension. *J. Fluid Mech.* **538**, 309–341.

Wiederseiner, S. 2010 Rheophysics of concentrated particle suspensions in a Couette cell using a refractive index matching technique. PhD thesis, Ecole Polytechnique Fédérale de Lausanne.

Wiederseiner, S., Andreini, N., Épely-Chauvin, G. & Ancey, C. 2011 Refractive index matching in concentrated particle suspensions: A review. *Exper. Fluids* **50**, 1183–1206.